Rolling element bearing condition monitoring using acoustic emission technique

F. Hemmati[1], **W. Orfali**[2], **M.S. Gadala**[1]
[1] University of British Columbia, Department of Mechanical Engineering
2324 Main Mall, Vancouver, B.C., Canada V6T-1Z4
e-mail: **gadala@mech.ubc.ca**

[2] Director of OMTC Chair & Acting Chairman, Civil Engineering Department, College of Engineering, Taibah University, Al Madina Al Munawara, Kingdom of Saudi Arabia

Abstract

Acoustic emission (AE) signals generated from defects in rolling element bearings are investigated analytically and experimentally in this paper. Roller element bearings are crucial parts of many machines and there has been an increasing demand for effective and reliable health monitoring of these data elements and for finding optimum procedures for the signal processing of the measured data to detect and diagnose the size and location of incipient defects in rolling element bearings. This paper describes a novel signal processing algorithm designed to diagnose localized defects on rolling element bearings components which has recently been tested for different operating speeds and loadings. The algorithm is based on optimizing the ratio of Kurtosis and Shannon entropy to obtain the optimal band pass filter utilizing wavelet packet transforms and envelope detection. Results show the superiority of the developed algorithm and its effectiveness in extracting bearing characteristic frequencies from the raw acoustic emission signals under different operating conditions. Also, the effects of defect size, operating speed, and loading conditions on AE burst duration have also been investigated to estimate the fault size on the outer race.

1 Introduction

Condition monitoring of heavy rotating machinery and equipment such as turbines, compressors and generators, is gaining importance in various industries since it keeps the plant at healthy condition for maximum production; helps in detecting faults at early stages; avoid serious accidents and damage; and reduces downtime. Bearings are the common elements used in heavy rotating machinery and equipment because of their high reliability. Bearings start to malfunction due to machine overload, shaft misalignment, rotor unbalance, overheating, etc. Many different techniques based on vibration methods have been developed to extract bearing fault features [1]. However, vibration signals are not sensitive to incipient faults and they usually masked by background noise caused by mechanical vibration signals from rotating machinery. Hence, it is normally difficult for the vibration techniques to detect bearing faults at an early stage.

Acoustic emission (AE) is the phenomenon of transient elastic wave generation due to a rapid release of strain energy caused by relative motion of small particles under mechanical stresses [2]. Interaction of rolling element bearing components and movement of bearing rollers over defects will produce AE's. The frequency content of acoustic emission (AE) is typically in the range of 100 kHz to 1 MHz, so AE is not influenced or distorted by imbalance and misalignment which are at low frequency ranges. The high sensitivity of AE technique and AE parameters in detecting the incipient bearing faults has become one of the significant advantages of AE over vibration measurement [3]. A comprehensive review of AE application for bearing fault detection was presented by Mba et al. [4]. Al-Ghamd and Mba [5] investigated the relationship between AE parameters in time domain and defect size. They concluded that AE burst duration is an effective parameter for identifying defect size on the outer race.

In order to effectively diagnose bearing faults on rolling element bearing components an advanced signal processing method is needed to enhance signal to noise ratio of AE signals. Dyer and Stewart [6] first presented the use of kurtosis parameter for bearing fault diagnosis and it was suggested to use kurtosis value in selected frequency bands. Antoni and Randall [7] presented the use of Spectral Kurtosis (SK) to extract transient components from a noisy signal. Sawalhi and Randall [8] proposed minimum entropy deconvolution (MED) technique along with SK to enhance the results of envelope analysis from a vibration bearing fault signal.

Wavelet transform (WT) has been used in signal denoising due to its high resolution in time and frequency domains [9]. For instance, Qiu [10] utilized wavelet filter-based denosing method to enhance weak periodic impulse signature masked by standard Gaussian white noise. However, WT cannot efficiently extract AE impulses from high freqeuncy bands where the bearing fault impulses exist [11]. Thus, wavelet packet transform (WPT) has been used to overcome this issue by decomposing a signal into different frequency bands [11]. Lei [12] proposed an improved kurtogram method for diagnosing bearing faults. Although, this method finds the frequency band which has the maximum value of kurtosis using WPT, wavelet function is not optimized in and kurtosis value does not provide any information regarding periodic behavior of bearing fault impulses.

In this paper, a new technique based on selecting the optimal band-pass filter using WPT is used in acoustic emission (AE) analysis to extract fault features. The outline of this paper is as follows: In Section 2, the concept of wavelet packet transform (WPT), Shannon entropy, and kurtogram are reviewed. In Section 3, the proposed method based on optimizing the kurtosis to Shannon entropy ratio of band-pass signal using WPT is discussed in detail. Then the effectiveness and underlying capability of proposed method in enhancing weak impulse signature is studied using a simulated signal. The results suggest that for impulse signals, the proposed method can select the optimal band-pass filter to detect periodic impulse signature which is completely masked by Gaussian white noise. In section 4, experimental setup is explained. In Section 5, the proposed method is applied to the experimentally acquired signals of a faulty bearing where the faults are artificially introduced on the outer race of the bearing. The results demonstrate that by selecting an optimal band-pass filter, bearing defects can be detected at an early stage of development. In this section, AE burst duration is also used to estimate the defect size on the outer race of a bearing.

2 Review of WPT, Shannon entropy, and Kurtogram

2.1 Wavelet packet transform

Wavelets are increasingly being used in signal processing and many engineering applications. Wavelets can be convoluted with portions of a transient signal to extract specific information from the signal at a given time. Unlike Fourier transform, which is frequency localized, wavelet transform (WT) technique may be used to decompose a transient signal into series of time-domain components, each covering a specific range. Therefore, WT has been widely used in signal processing and signal de-noising due to its extraordinary time-frequency or more properly term time-scale representation capability. The continuous wavelet transform of finite-energy signals ($f(t) \in L^2(r)$) with the analyzing wavelet (mother wavelet function) $\psi(t)$, is the convolution of $f(t)$ with a scaled and conjugated wavelet:

$$W_f(a,b) = \int_{-\infty}^{+\infty} f(t) \frac{1}{\sqrt{a}} \psi^* \left(\frac{t-b}{a} \right) dt \tag{1}$$

where $\psi^*(t)$ stands for the complex conjugation of $\psi(t)$. In the above equation a and b are the dilation and translation, respectively, which may be continuous or discrete. The factor $\frac{1}{\sqrt{a}}$ is used for energy preservation. Equation (1) indicates that the wavelet transform is a time-scale analysis. The wavelet transform can also be considered as a filtering operation by changing a and b to obtain frequency segmentation. By replacing a and b with 2^{-j} and $2^{-j}k$ respectively, where k and j are integer values, the discrete wavelet can be written as,

$$W_f(j,k) = \sqrt{2^j}\int_{-\infty}^{+\infty} f(t)\,\psi^*(2^j t - k)dt \tag{2}$$

Discrete form of wavelet transform can be implemented by using filter $h(k)$and $g(k)$ which are low-pass filter related to the scaling function $\phi(t)$ and high-pass filter related to wavelet function (t), respectively.

$$\phi_j(t) = \sum_k h(k) 2^{(j+1)/2}\phi(2^{j+1}t - k) \tag{3}$$

$$\psi_j(t) = \sum_k g(k) 2^{(j+1)/2}\phi(2^{j+1}t - k) \tag{4}$$

The basic step of discrete wavelet transform is illustrated in Figure 1. The signal s is convolved with a low pass filter L and a high pas filter H. Decomposition outcomes, cA_1 and cD_1 are called approximate coefficients and detailed coefficients, respectively. The symbol ↓2 denotes down sampling.

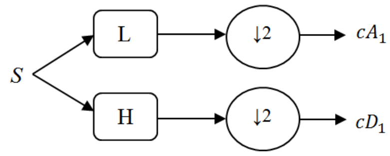

Figure 1: Basic step of decomposition of wavelet transform

The wavelet packet transform is a generalization of the wavelet transform and it has been used in signal processing of vibration and acoustic emission signals [13]. WPT can be implemented based on wavelet filters. Thus, WPT coefficients at each level are defined by following equations:

$$W_{j+1}^{2K} = W_j^K(n) * h(-2n) \tag{5}$$

$$W_{j+1}^{2K+1} = W_j^K(n) * g(-2n) \tag{6}$$

where W_{j+1}^{2K} denotes the jth decomposed level of wavelet packet coefficient at frequency band of $2k$ $(0 < k < 2^j - 1)$; $h(-2n)$ and $g(-2n)$ are the low-pass and high-pass filters, respectively based on the selected wavelet function. In practice a fast algorithm is applied by splitting approximations and details into finer components. Therefore, wavelet packet transform is more efficient than wavelet transform of the time-scale analysis to describe bearing fault signal in different frequency bands of local information.

The proposed method uses the WPT as a powerful tool to do orthogonal decomposition of AE signals in the whole frequency domain. As a result, wavelet packet transform (WPT) can process all frequency bands, especially high frequency bands, more efficiently where bearing characteristic frequencies exist.

2.2 Shannon entropy

Entropy is a common idea in many fields, especially in signal processing and condition monitoring [14]. Adding a very small noise to a signal will cause a significant change in the amount of entropy. Shannon entropy H of a discrete random variable X with possible values $\{x_1, x_2, \dots, x_n\}$ can be written as [15],

$$H(X) = -\sum_{i=1}^{n} p(x_i)\log(p(x_i)), \quad \sum_{i=1}^{n} p(x_i) = 1 \tag{7}$$

where p is the probability mass function of random variable X. In information theory or statistical measurement, Shannon entropy is sometimes referred to as a measure of information loss of a random variable [16]. Shannon entropy of a normalized signal measures the amount of randomness and sparseness of data. Thus, a signal with minimal amount of Shannon entropy can be treated as the most periodic and greatest amount of signal to noise ratio. In the present study Shannon entropy has been used as a measure of periodicity of signals in different frequency bands. When roller elements pass over a defect on bearing components, a series of AE impulses will be generated. These impulses repeat at a specific frequency, hence, the signal frequency band produced by WPT which has the minimum value of entropy contains the maximum periodicity and signal to noise ratio.

2.3 Kurtogram

Kurtosis characterizes the relative peakedness or flatness of a distribution of measured values. A high kurtosis distribution has a sharper peak and longer tail; however, low kurtosis distribution has smoother and curvier peak and thinner tail. Kurtosis has been used as a measure of the severity of machine faults since it was introduced by Dyer & Stewart [6].

$$Kurtosis = \frac{(N)\sum_{i=1}^{N}(x_i - \bar{x})^4}{\left(\sum_{i=1}^{N}(x_i - \bar{x})^2\right)^2} \tag{8}$$

Spectral kurtosis (SK) was first used by Dwyer [17] for detecting impulsive events in sonar signals. It was based on the short time Fourier transform (STFT) and measures impulsiveness of a signal as a function of frequency. Also, SK has been used to identify the presence of non-Gaussian components due to bearing faults and to indicate in which frequency range it may occur. This may be utilized to discover the presence of transients in a signal and for finding their locations in the frequency domain. A thorough review of the subject and its application to condition based health monitoring and machine fault diagnosis may be found in [18]. Based on Wold-Cramér decomposition of a non-stationary signal, the signal $X(t)$, as a response of a system, for the case of a series of impulses $h(t)$, which can be a model of a rolling element bearing signal, excited by $Z(t)$ can be written as [18],

$$X(t) = \int_{-\infty}^{+\infty} e^{i2\pi ft} H(t,f)\, dZ(f) \tag{9}$$

where $dZ(f)$ is an orthonormal spectral increment and $H(t,f)$ is the complex envelope of $X(t)$ at frequency f. The SK can be defined by taking the fourth power of $H(t,f)$ at each time and averaging its value along the record and normalizing it by the square of the mean square value. It can be proved that if 2 is subtracted from this ratio, as given in Eq.(10), the result will be zero for a Gaussian signal [18]:

$$K(f) = \frac{\langle H^4(t,f)\rangle}{\langle H^2(t,f)\rangle^2} - 2 \tag{10}$$

Spectral kurtosis (SK) is proved as an effective tool which can locate frequency bands with a high amount of impulsiveness, and also for filtering out the signal to maximize peakendness. Thus, kurtosis will be high if the filtered signal has separated impulses which can be regarded as bearing characteristic frequency. Antoni [18] computed the STFT-based SK for different window lengths to calculate the window length which maximizes the overall level of the SK in the selected frequency band. This technique was investigated in detail, and led to the concept of the ‘‘kurtogram’’, which is a two dimensional map and presents optimum central frequency (f) and bandwidth (Δf) where kurtosis value is maximum. The problem of this technique is kurtogram does not provide any information regarding periodicity of a signal at each frequency band. A detailed information and fast computational of kurtogram is presented in [19].

3 Proposed method

Local defects on the roller element bearing components cause periodic impulses in AE signals. AE impulses may be masked and distorted by the background noise. Thus, the frequency band which contains a signal with maximum periodicity and signal to noise ratio can be regarded as the optimal band-pass filter. In this study, first, best wavelet function is selected based on minimizing the Shannon entropy of reconstructed signal. Thus, the original AE signal is reconstructed utilizing DMeyer, Daubechies, Symlets, and Coiflets to investigate which wavelet function minimizes the Shannon entropy of the reconstructed signal. Second, the wavelet packet transform is implemented on the acoustic emission (AE) signal, and thus, different frequency-band signals are produced according to the WPT decomposition level. Third, the value of kurtosis to entropy ratio (KER) is calculated for each of pre-normalized signals from WPT frequency-bands. The WPT decomposition of a signal with a sampling frequency of 2π utilizing kurtosis to Shannon entropy (KER) for three level of decomposition is shown in Figure 2. Forth, frequency band which has the maximum value of KER is selected as an optimal band-pass filter since it contains characteristic fault frequencies. Fifth, envelope spectrum using Hilbert transform along with FFT is constructed to diagnose characteristic defect frequencies of faulty bearing. The flow chart of the proposed method can be shown in Figure 3. As mentioned above optimal frequency-band signal is selected based on:

- High sensitivity of kurtosis value to impulses which are attributed to AE pulses caused by movement of rolling element components over localized defects.
- High sensitivity of Shannon entropy to fault periodic pattern and signal to noise ratio.

Therefore the proposed method can simply extract a band-pass filtered signal, even with small signal to noise ratio, which contains fault features.

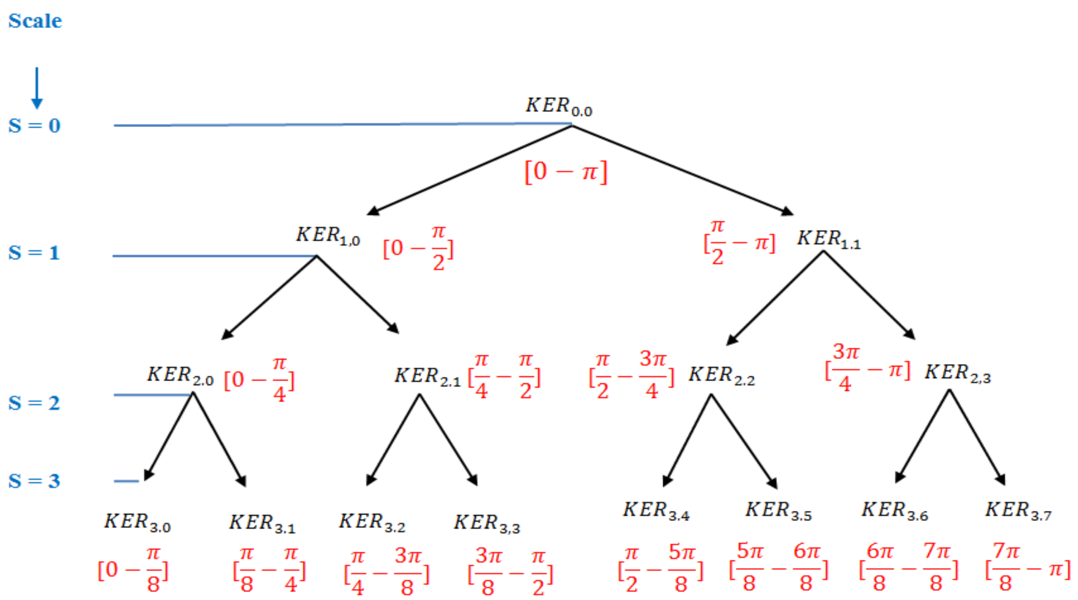

Figure 2: Three level decomposition of wavelet packet transform (WPT)

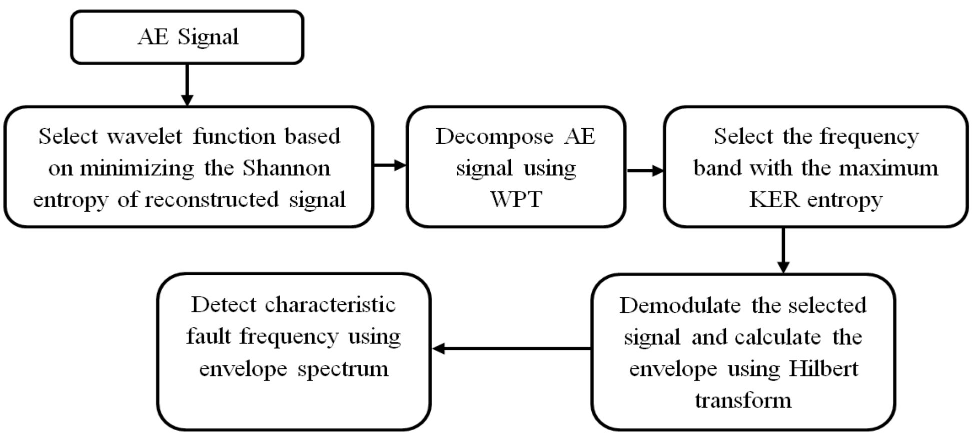

Figure 3: Flow chart of the proposed method.

3.1 De-noising the simulated signal using the proposed method

In order to observe the effectiveness of the proposed method, this method is applied to a sample of simulated data. Simulated data from [20] with simple modification is used to simulate faulty bearings. Simulated signal is illustrated in Figure 4.

$$g_i(t) = \begin{cases} A_i e^{-\alpha(t-\frac{i}{F})} \sin\left(2\pi f(t-\frac{i}{F})\right) & if\ (t-\frac{i}{F}) > 0 \\ 0 & if\ (t-\frac{i}{F}) < 0 \end{cases} \tag{11}$$

where A_i is amplitude of ith impulse and N is number of impulses which is assumed to be random. F, f, and α are the characteristic fault frequency, excited resonance frequency and decay parameter, respectively. Simulated signal can be written as,

$$S(t) = \sum_{i=1}^{N} g_i(t) + Z(n) \tag{12}$$

where $g_i(t)$ is ith impulse and *Z(n)* is Gaussian white noise which is added to the original data to produce a noisy signal of *S*(t). In this paper, sampling frequency and characteristic fault frequency of a simulated signal of faulty bearing are set to 20 kHz and 4 Hz, respectively, and all parameters are given in Table 1.

Parameters	A_i	i	F	f	α
Values	random	16	4Hz	2000 Hz	80

Table 1: Simulated bearing fault parameters

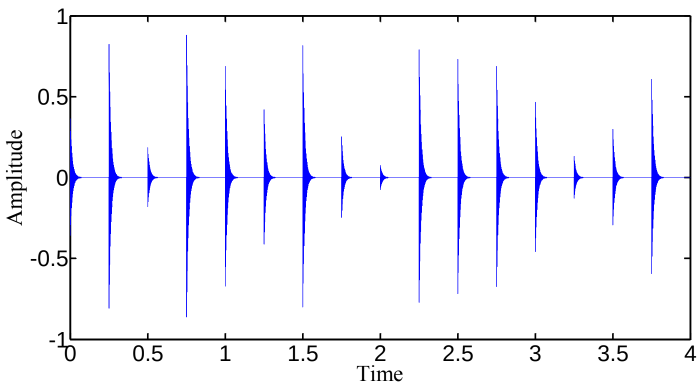

Figure 4: Simulated impulse signal

To examine the performance of the proposed method, signal to noise ratio (SNR) of -20 dB is selected in Figure 5(a) to simulate an extremely noisy bearing fault signal. From the envelope spectrum of the noisy signal shown in Figure 5(b) no information can be obtained. It is observed that defect frequencies completely masked by noise and there is no evident of fault frequencies. This means that the envelope spectrum fails to extract characteristic frequencies from a noisy signal. Wavelet selection method is applied to diagnose the best wavelet function. Daubechies wavelet (db43) is selected as the best wavelet function which minimizes the Shannon entropy of the reconstructed signal. Then the proposed method is implemented using WPT along with KER calculation of each frequency band signal to detect the optimal band-pass filter which is shown in Figure 6. It is shown that the maximum value of KER is at the seventh decomposition level which is node number 148 of WPT tree. The frequency band signal which is shown in Figure 7(a) reveals clear impulses. Characteristic frequency of 4 Hz and its harmonics are obvious from the envelope spectrum of frequency band signal in Figure 7(b).

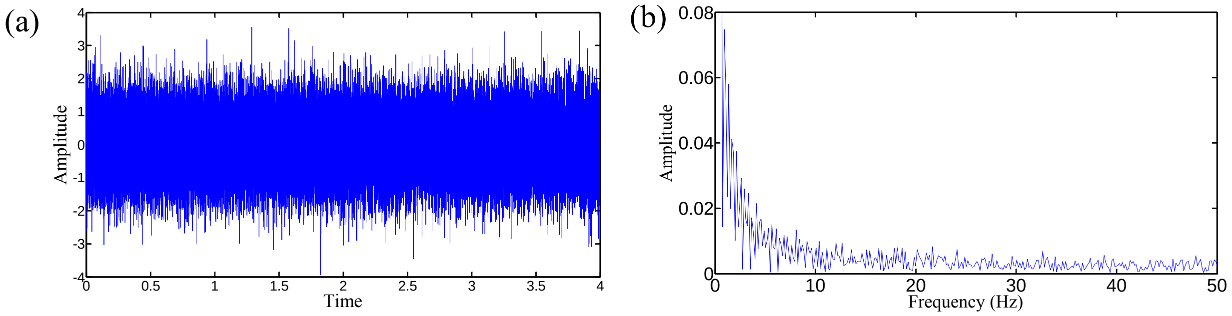

Figure 5: (a) simulated impulse signal with noise (SNR = -20 dB), (b) envelope spectrum of the simulated signal

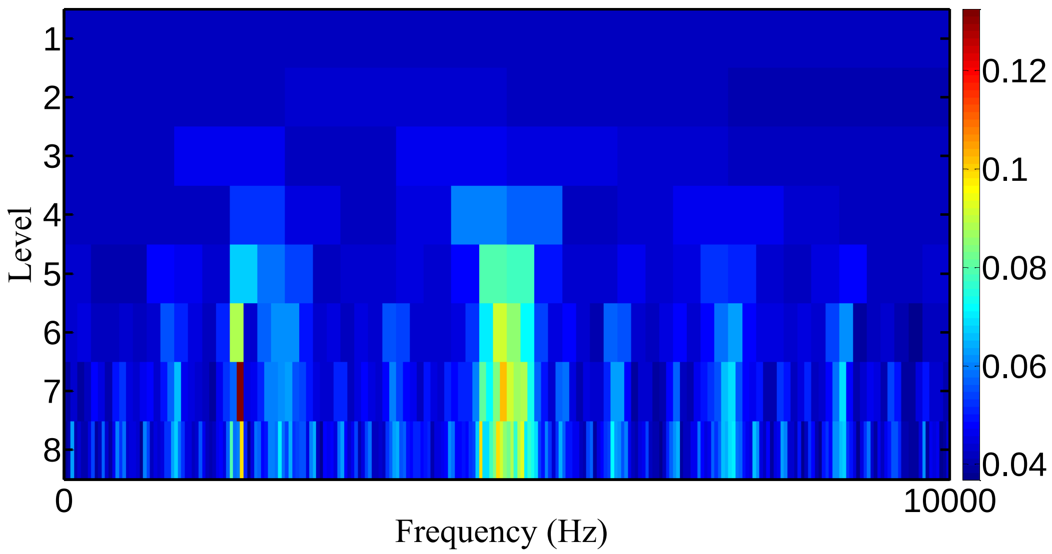

Figure 6: WPT and KER calculations of the simulated bearing fault signal

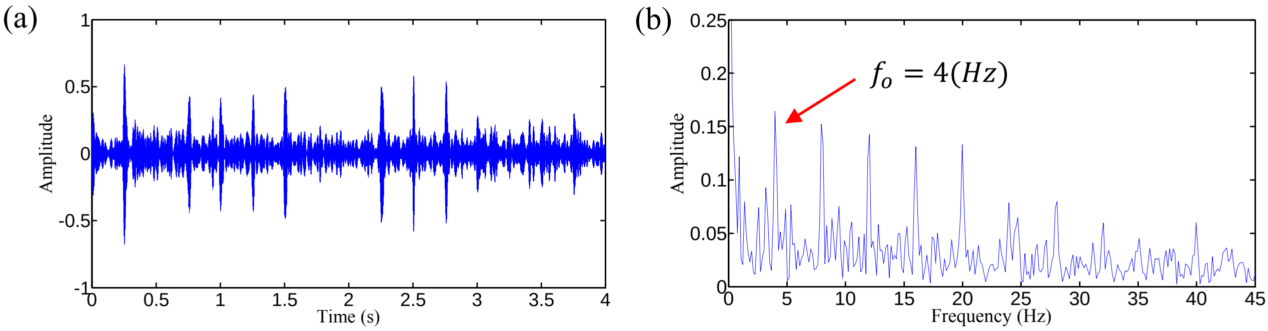

Figure 7: (a) Frequency band signal (de-noised signal), (b) envelope spectrum of de-noised signal

4 Experimental setup

The experimental setup is consisted of a spindle, driven by a variable speed motor and a dismountable bearing test rig which is shown in Figure 8(a) and (b). The spindle can be driven from 130 rpm up to 2200 rpm. A 09074 separable Timken tapered roller bearing is mounted on a pillow block in order to enhance the feasibility of introducing faults on the outer race and roller elements, moreover, assembly and disassembly of the bearing was accomplished with minimum disruption to the test setup. Bearing parameters are tabulated in Table 2.

Bearing specification	Timken 09074
Ball diameter (BD)	7.2 (mm)
Pitch diameter (PD)	33.5 (mm)
Number of rollers (n)	12
Contact angle (β)	0

Table 2: Bearing parameters

A second bearing was mounted in the middle of the shaft, which supports variable radial loads. The load was measured using load cell 247AS which has a capacity of 2000 N. The AE data acquisition and sensor used for the bearing fault diagnosis were NI and Physical Acoustic testing system respectively. The AE sensor (Nano-30 Physical Acoustic) was placed on the top of the bearing pillow block. The AE signals detected by the sensor were gained for 20 dB and all-pass filtered by the pre-amplifier (PAC 2/4/6c). The preprocessed signal is digitized by NI USB-6366 for data sampling at variable frequencies. 5 data files were recorded for each experimental test.

(a)

(b)

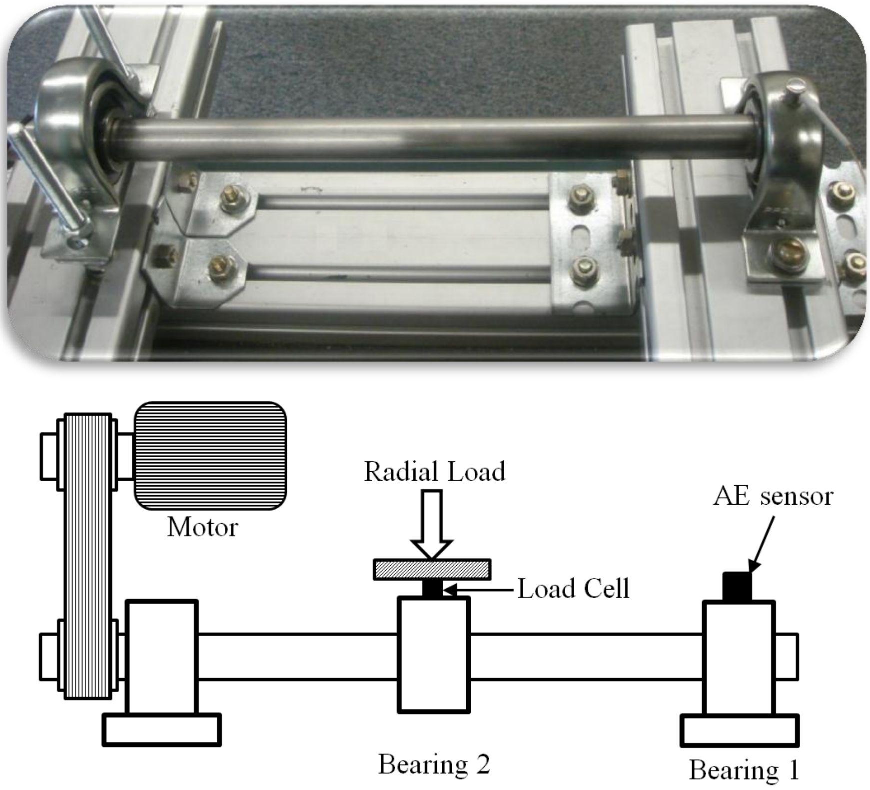

Figure 8: (a) Experimental test setup, (b) experimental setup sketch

5 Experimental results

5.1 Characteristic fault frequencies of a bearing with a line defect

The experimental tests for diagnosing the characteristic fault frequencies were carried out using a faulty bearing with an outer race line defect shape. Localized defect was seeded on the race by an engraving tooling machine to keep the size and depth under control. The size of the artificial line defect was 1mm in width and 0.5mm in depth which is shown in Figure 9.

In a faulty bearing, defects at different locations (inner race, outer race, and roller) have characteristic fault frequencies at which bursts occur. Therefore, an AE signal of a defective bearing consists of periodic events at a corresponding characteristic fault frequency. Assuming a bearing with a fixed outer race, the characteristic defect frequency of outer race can be theoretically calculated as follows [3]:

$$f_{or} = \frac{n}{2} f_r \left(1 - \left(\frac{BD}{PD}\right) \cos \beta\right) \tag{13}$$

where BD and PD are roller diameter and bearing pitch diameter, respectively. f_r is the shaft rotating speed, β is the contact angle between the outer race and the ball, and n is the number of roller elements. For speeds up to 2200 rpm, outer race defect frequencies lie in the low-frequency range (Less than 200Hz). However, in reality, due to slipping in the rolling element bearings, outer race characteristic frequency may be slightly different from its calculated value [21]. By comparing the measured characteristic frequency and the theoretical frequency, location of the defect can be identified.

Figure 9: Pictures of faulty bearing components with line shape defect on the outer race

For the results reported in this section, measured AE signals were all sampled at a rate of 500 kHz and a total number of 1,500,000 (3 seconds) data points were recorded. The AE signals have been acquired under conditions of (S300, L0), (S300, L300), (S2200, L0), and (S2200, L300) are illustrated in Figure 10. As it can be seen in Figure 10 the intensity of AE signals increases by applying higher radial loads, while the quality of all the signals are affected by the presence of noise. The WPT along with KER calculation at each frequency band is applied on the AE signals which are shown in

Figure 11. The maximum KERs for each condition are indicated by the black rectangles. By comparing the maximum KERs at different speeds, it can be concluded that at low speeds bearing fault impulses are more localized at low frequencies, however, at high speeds they are more shifted to the high frequencies. The results for the best wavelet function based on minimizing the Shannon entropy of reconstructed signal and optimal band-pass filter are summarized in Table 3.

Condition	Best Wavelet Function	Optimal Frequency Band (Hz)	Level
S300, L0	db39	7812.5-15625	5
S300, L300	db44	27343.75-29296.875	7
S2200, L0	db42	125000- 132812.5	5
S2200, L300	db39	125000- 132812.5	5

Table 3: Optimal wavelet function and frequency bands for each condition

The successful enhancement of the features in the AE signals can be verified by direct comparison of the results shown in Figure 10 and 12. The envelope spectrum, using Hilbert transform, of filtered signals clearly show the bearing fault frequencies and their harmonics Figure 13.

The measured fault frequencies and theoretical values are summarized in Table 4. The maximum deviation of the measured frequencies from the calculated theoretical values does not exceed than 3% error which is again an indication of the applicability and preciseness of the proposed method.

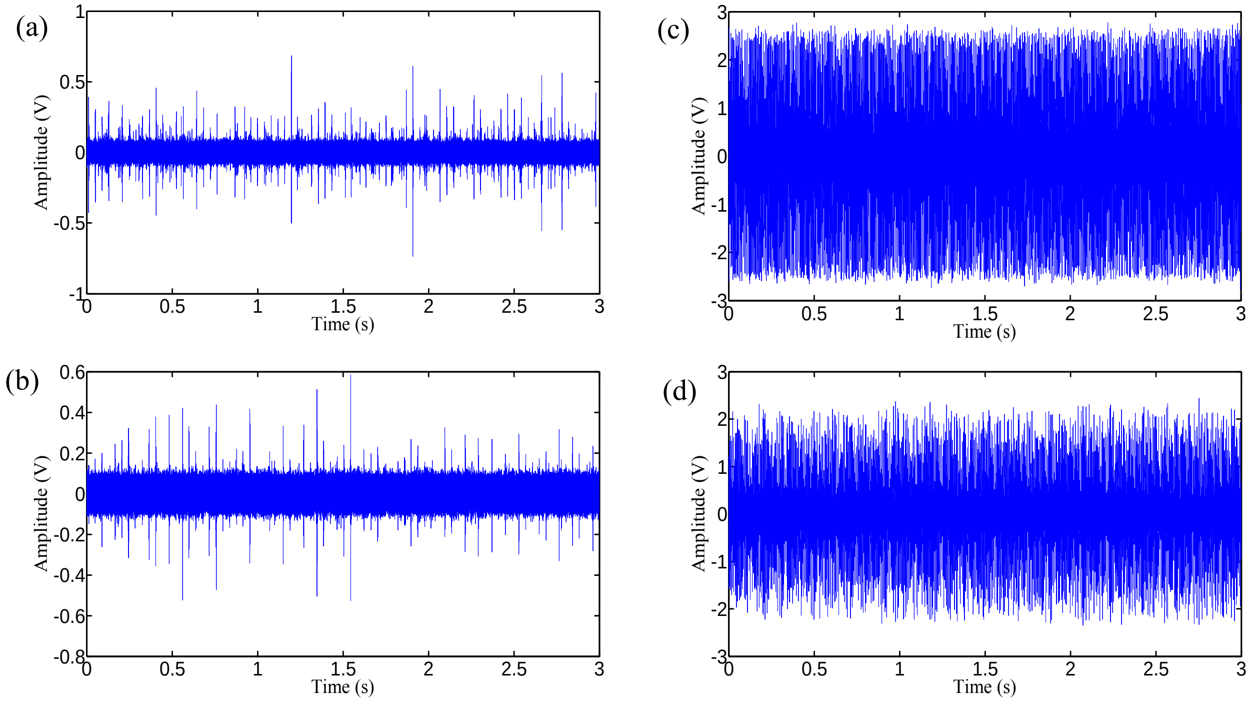

Figure 10: AE signals from the bearing with an outer race line shape defect, (a) condition (S300, L0), (b) condition (S300, L300N), (c) condition (S2200, L0), and (d) condition (S2200, L300)

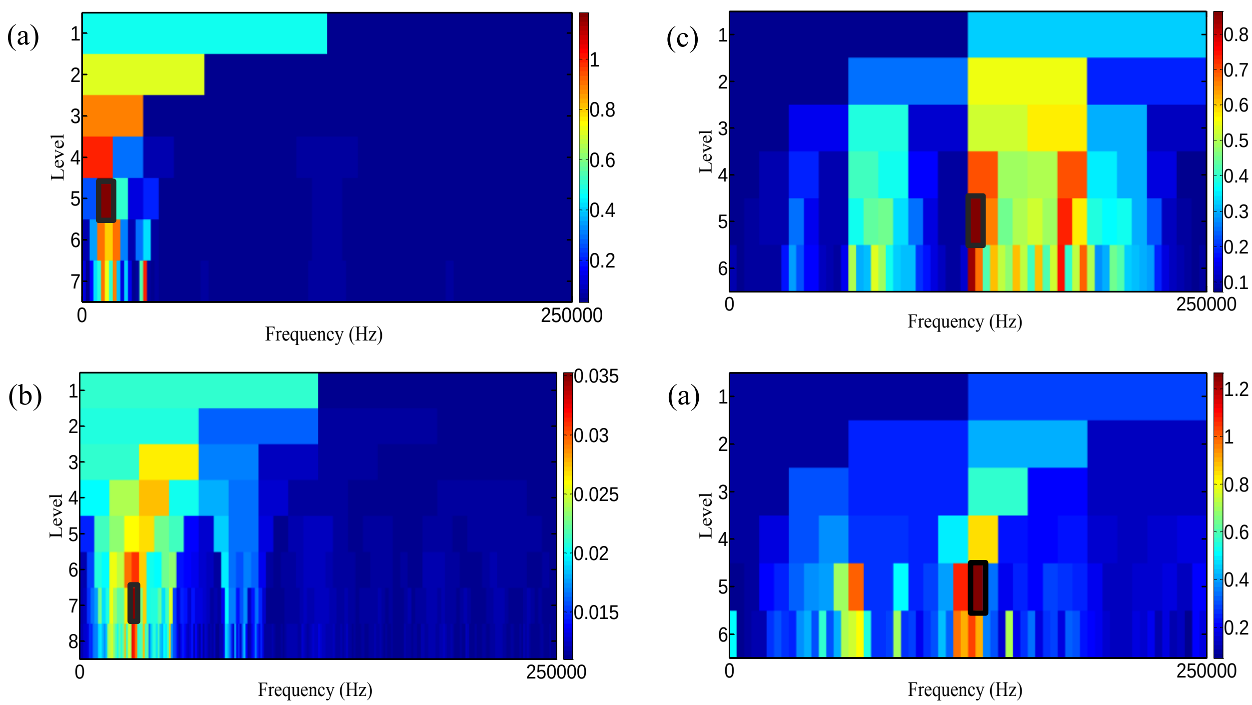

Figure 11: WPT and KER calculations of AE signals, (a) condition (S300, L0), (b) condition (S300, L300N), (c) condition (S2200, L0), and (d) condition (S2200, L300)

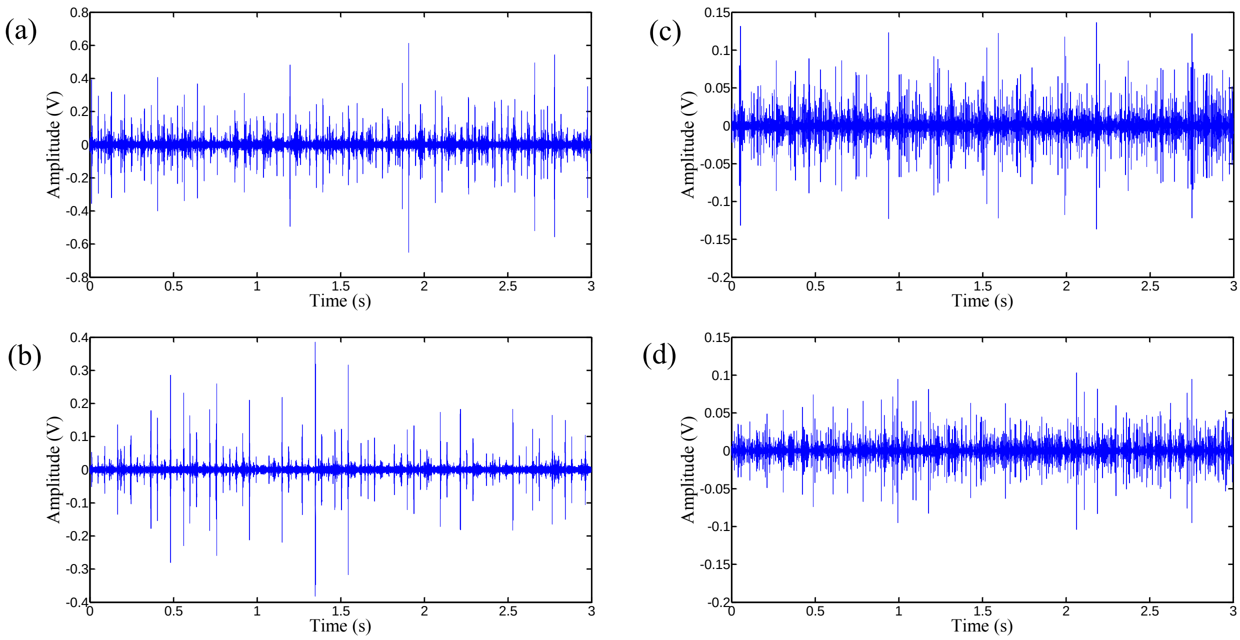

Figure 12: De-noised AE signals using WPT and KER calculations, (a) condition (S300, L0), (b) condition (S300, L300N), (c) condition (S2200, L0), and (d) condition (S2200, L300)

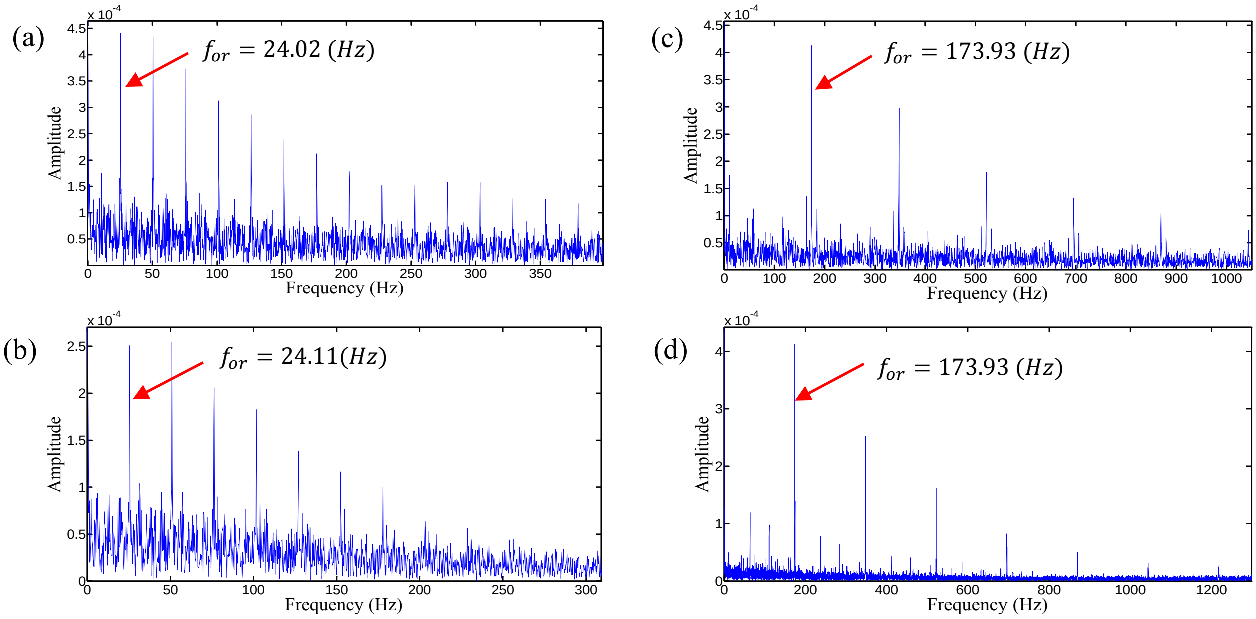

Figure 13: Envelope spectrum of de-noised AE signals, (a) condition (S300, L0), (b) condition (S300, L300N), (c) condition (S2200, L0), and (d) condition (S2200, L300)

Condition	Theoretical Frequency (Hz)	Measured Frequency (Hz)	Error (%)
S300, L0	23.55	24.02	2
S300, L300	23.55	24.11	2.4
S2200, L0	172.72	173.93	1
S2200, L300	172.72	173.93	1

Table 4: Characteristic fault frequency analysis

5.2 Defect size calculation

After successfully characterizing the fault frequencies, the new goal is to find the actual defect size by means of studying the AE burst duration of measured signals. In this section AE signals were sampled at a rate of 2MHz. The size of the artificial line shape defects were 1mm (D1) and 2mm (D2) in width and 0.5mm in depth. For measured AE signals the experiments were conducted at speeds of 600 rpm (S600) and 1100 rpm (S1100) and under loads of 0 N (L0) and 300 N (L300) to investigate the effects of speed and load on the AE burst duration. For the cases when the speed is set to 600rpm (S600), 5 individual AE bursts can be detected in the selected time window, while, 9 AE bursts can be identified for the case of S1100. Any specific defect is associated with a unique AE transient burst duration. The start of this duration is identified with the point which the AE response is higher than the underlying background noise level. The end of the AE burst duration is selected at the point which the response falls below the underlying noise level. After the AE burst durations are successfully found, the arithmetic mean of all AE bursts is calculated and reported as the experimentally measured AE burst duration. An example of AE measured waveforms and its corresponding burst durations is shown in Figure 14. AE burst durations under different conditions is illustrated in Figure 15. As it can be seen from Figure 15, it can be concluded that the AE burst duration of measured data is not sensitive to the loading condition of the bearing, while the effect of increasing the speed is clearly demonstrated.

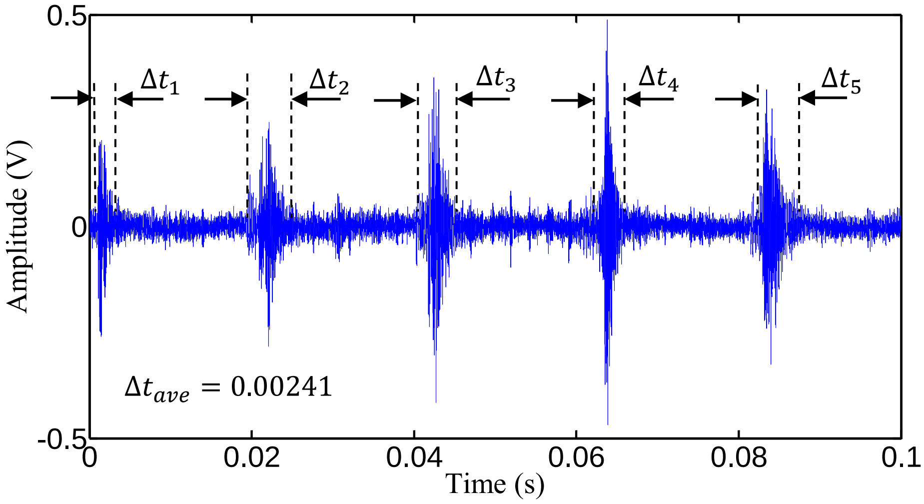

Figure 14: Example procedure of determining the AE burst duration in condition (S600, L300, D1)

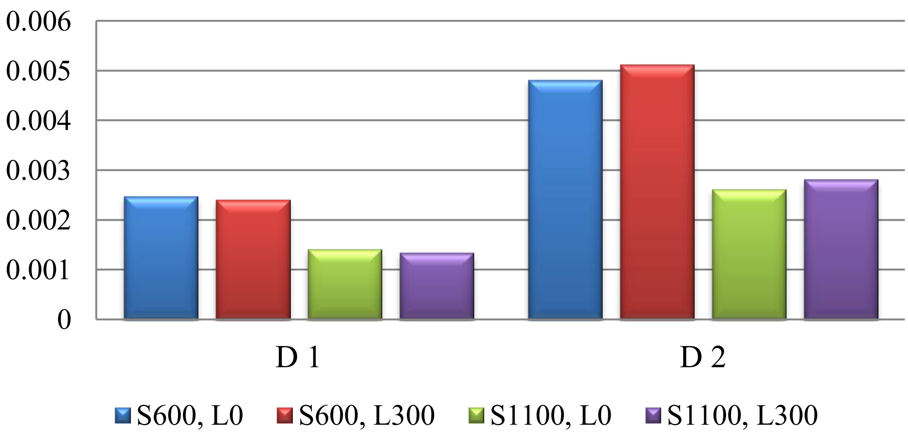

Figure 15: Comparison of AE burst duration for various conditions

The theoretical time travel duration of roller elements passing over a defect on the outer race can be calculated based on shaft rotating speed and relative velocities of outer race and roller elements. The objective is to correlate the theoretical and measured AE burst duration. The schematic of bearing components with an outer race defect is shown in Figure 16. The relative velocity of roller elements and the outer race is known as cage frequency which is given by [3],

$$f_c = \frac{f_r}{2}\left(1 - \left(\frac{BD}{PD}\right) COS\ \beta\right) \tag{14}$$

where PD and BD are pitch diameter and ball diameter of rolling element bearing respectively. f_r is the shaft rotating speed in (rad/s) and β is the contact angle which is assumed to be zero theoretically.

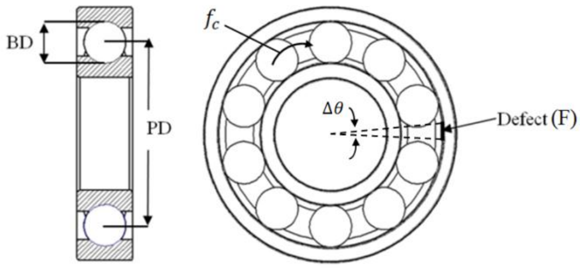

Figure 16: Schematic of bearing components with an outer race defect

A typical line defect on the outer race of a bearing can be represented both with its length or an associated angle. This angle can be calculated by measuring the angle between the lines connecting the center of the bearing to the either side of the line fault as follows:

$$\Delta\theta = \frac{f_r}{2}\left(1 - \left(\frac{BD}{PD}\right)\right)\Delta t = \frac{2F}{(PD + BD)} \tag{15}$$

where F is defect size and Δt is time travel duration of roller elements. The above equation can be simplified into the compact form of:

$$\Delta t = \frac{4F(PD)}{f_r(PD^2 - BD^2)} \tag{16}$$

Theoretically calculated time travel durations and experimentally obtained AE burst durations are tabulated in Table 5 and Table 6 for comparison purposes. As it can be seen from Table 5 and 6 the relative error does not exceed 30% in any case. It shall be noted that one major source of the deviation in experimentally found values of the AE burst duration compared to the theoretically obtained ones is due to unrealistic assumption of no slip condition between roller element bearing components that is used to derive the theoretical equation.

Speed (rpm)	Theory (sec)	Experiment (sec)		Error %	
		L0	L300	L0	L300
600	0.002	0.00248	0.00241	24	20.5
1100	0.0011	0.00141	0.00134	28.18	21.82

Table 5: Experimental and theoretical AE burst duration for D1

Speed (rpm)	Theoretical (sec)	Experiment (sec)		Error %	
		L0	L300	L0	L300
600	0.004	0.00482	0.00513	20.5	28.25
1100	0.0022	0.00262	0.00281	19.1	27.73

Table 6: Experimental and theoretical AE burst duration for D2

6 Conclusion

Feature enhancement of the weak signature from the noisy signal is essential to fault prognostics, in which case features are often very weak and masked by the background noise.

This paper presents a new approach of optimizing wavelet functions based on minimizing the Shannon entropy of reconstructed signal, and selecting the optimal band pass filter signal using KER calculation of WPT band-pass signals to detect bearing faults.

This method is well suited for detecting the weak signature from a defective bearing signal where defect features are impulse-like. The simulated bearing fault signal which was completely masked by the noise was enhanced and the characteristic frequency was successfully detected using envelope spectrum. Also, experimental results verified the effectiveness of the proposed method by measuring the fault frequency on the outer race under varying the rotational speeds and loadings. The weak periodic impulse signatures were successfully enhanced and experimental fault frequencies compared with their theoretical values which revealed the maximum error of 3%.

To estimate the defect size, AE burst duration of the measured signals compared with their theoretical values which shown errors did not exceed 30%. AE burst durations are not sensitive to the loading conditions and by increasing the defect size the AE burst durations increased. Thus, AE burst duration can be a powerful tool to estimate the defect size on the outer race under different loading conditions and speeds.

References

[1] P. McFadden and J. Smith, "Model for the vibration produced by a single point defect in a rolling element bearing," *Journal of Sound and Vibration,* vol. 96, pp. 69-82, 1984.

[2] Y. H. Pao, R. R. Gajewski, and A. N. Ceranoglu, "Acoustic emission and transient waves in an elastic plate," *The Journal of the Acoustical Society of America,* vol. 65, p. 96, 1979.

[3] N. Tandon and A. Choudhury, "A review of vibration and acoustic measurement methods for the detection of defects in rolling element bearings," *Tribology International,* vol. 32, pp. 469-480, 1999.

[4] D. Mba and R. B. K. N. Rao, "Development of Acoustic Emission Technology for Condition Monitoring and Diagnosis of Rotating Machines; Bearings, Pumps, Gearboxes, Engines and Rotating Structures," 2006.

[5] A. M. Al-Ghamd and D. Mba, "A comparative experimental study on the use of acoustic emission and vibration analysis for bearing defect identification and estimation of defect size," *Mechanical Systems and Signal Processing,* vol. 20, pp. 1537-1571, 2006.

[6] D. Dyer and R. Stewart, "Detection of rolling element bearing damage by statistical vibration analysis," 1977.

[7] J. Antoni and R. Randall, "The spectral kurtosis: application to the vibratory surveillance and diagnostics of rotating machines," *Mechanical Systems and Signal Processing,* vol. 20, pp. 308-331, 2006.

[8] N. Sawalhi, R. Randall, and H. Endo, "The enhancement of fault detection and diagnosis in rolling element bearings using minimum entropy deconvolution combined with spectral kurtosis," *Mechanical Systems and Signal Processing,* vol. 21, pp. 2616-2633, 2007.

[9] C. Yiakopoulos and I. Antoniadis, "Wavelet based demodulation of vibration signals generated by defects in rolling element bearings," *Shock and Vibration,* vol. 9, pp. 293-306, 2002.

[10] H. Qiu, J. Lee, J. Lin, and G. Yu, "Wavelet filter-based weak signature detection method and its application on rolling element bearing prognostics," *Journal of Sound and Vibration,* vol. 289, pp. 1066-1090, 2006.

[11] J. Zarei and J. Poshtan, "Bearing fault detection using wavelet packet transform of induction motor stator current," *Tribology International,* vol. 40, pp. 763-769, 2007.

[12] Y. Lei, J. Lin, Z. He, and Y. Zi, "Application of an improved kurtogram method for fault diagnosis of rolling element bearings," *Mechanical Systems and Signal Processing,* 2011.
[13] Y. Wu and R. Du, "Feature extraction and assessment using wavelet packets for monitoring of machining processes," *Mechanical Systems and Signal Processing,* vol. 10, pp. 29-53, 1996.
[14] J. D. Wu and C. H. Liu, "An expert system for fault diagnosis in internal combustion engines using wavelet packet transform and neural network," *Expert Systems with Applications,* vol. 36, pp. 4278-4286, 2009.
[15] C. E. Shannon, "A mathematical theory of communication," *ACM SIGMOBILE Mobile Computing and Communications Review,* vol. 5, pp. 3-55, 2001.
[16] S. Ihara, *Information theory for continuous systems* vol. 2: World Scientific Pub Co Inc, 1993.
[17] R. Dwyer, "Detection of non-Gaussian signals by frequency domain kurtosis estimation," 1983, pp. 607-610.
[18] J. Antoni, "The spectral kurtosis: a useful tool for characterising non-stationary signals," *Mechanical Systems and Signal Processing,* vol. 20, pp. 282-307, 2006.
[19] J. Antoni, "Fast computation of the kurtogram for the detection of transient faults," *Mechanical Systems and Signal Processing,* vol. 21, pp. 108-124, 2007.
[20] S. Ericsson, N. Grip, E. Johansson, L. E. Persson, R. Sjöberg, and J. O. Strömberg, "Towards automatic detection of local bearing defects in rotating machines," *Mechanical Systems and Signal Processing,* vol. 19, pp. 509-535, 2005.
[21] H. Prashad, "The effect of cage and roller slip on the measured defect frequency response of rolling-element bearings," *ASLE TRANSACTIONS,* vol. 30, pp. 360-367, 1987.